

Supporting Information

Heterostructured Ferroelectric BaTiO₃@MOF-Fe/Co Electrocatalysts for Efficient Oxygen Evolution Reaction

Shuang Wang^{†,1}, Qiong Li^{‡,1}, Shujuan Sun[†], Kai Ge[†], Yi Zhao[†], Kai Yang[†], Zhiheng Zhang[†], Jiayu Cao[†], Jie Lu[†], Yongfang Yang^{†*}, Yue Zhang^{†*}, Mingwang Pan^{†*}, Zhiqun Lin^{§*}, Lei Zhu^{‡*}

[†] *Institute of Polymer Science and Engineering, Hebei Key Laboratory of Functional Polymers, Hebei University of Technology, Tianjin 300130, P. R. China*

[‡] *Department of Macromolecular Science and Engineering, Case Western Reserve University, Cleveland, Ohio 44106-7202, United States*

[§] *School of Materials Science and Engineering, Georgia Institute of Technology, Atlanta, Georgia 30332, United States*

* Emails: yyf@mail.nankai.edu.cn (Y. Yang), zylizzy@126.com (Y. Zhang), mwpan@126.com (M. Pan), zhiqun.lin@mse.gatech.edu (Z. Lin), lxz121@case.edu (L. Zhu)

¹ These authors have equal contributions to the work and should be considered co-first authors.

1. Experimental section

1.1 Materials

BaTiO₃ NPs with various sizes were purchased from U.S. Research Nanomaterials, Inc. (Houston, TX). The as-received BTO (arBTO) NPs was thermally annealed at 950 °C in air for 72 h to obtain annealed BTO (anBTO) NPs. This temperature was chosen because no significant sintering was observed when the particle size was above 200 nm. N,N-dimethylformamide (DMF) was purchased from Tianjin Sailboat Chemical Reagent Technology Co., Ltd. Succinic anhydride was purchased by Tianjin No. 1 Chemical Reagent Factory. (3-Aminopropyl)triethoxysilane (KH-550) was acquired from Chengdu Kelong Chemical Reagent Factory. Iron chloride hexahydrate (FeCl₃·6H₂O, 99.99%) and cobalt nitrate hexahydrate [Co·(NO₃)₂·6H₂O, 99.99%] were purchased from Sinopharm Chemical Reagent Co., Ltd. 1,4-BDC, Nafion solution (0.05 wt.%), and potassium hydroxide (KOH, 95%, AR grade) were purchased from Alfa Aesar. TEA was obtained from Tianjin Fuchen Chemicals Reagent Factory. The Smooth-On Ecoflex 00-30 two-component silicone rubber was purchased from Amazon. All other reagents were analytical grade and used directly without further purification.

1.2 Preparation of surface-carboxylated BaTiO₃ NPs

0.5 mL of KH-550 (6.4 mmol) was added dropwise to a 20 mL DMF solution containing succinic anhydride (0.30 g, 3 mmol). After the mixture was stirred at room temperature for 3 h, N-[3-(triethoxysilyl)propyl]-4-carboxylbutanamide (R-KH550) was generated. Then, 0.10 g of arBTO or anBTO NPs dispersed in a mixture solvent (1 mL of deionized water and 5 mL of DMF) was added. After stirring for 8 h at room temperature, the solid powder was obtained via centrifugation at 5000 rpm. The carboxylated BaTiO₃ NPs (Scheme 1) were sequentially washed with distilled water and ethanol for three times. Finally, the products were dried under vacuum at 60 °C overnight and stored in a desiccator before use.

1.3 Synthesis of BaTiO₃/MOF heterostructures

Carboxylated BaTiO₃ NPs (30 mg), 12 mg of FeCl₃·6H₂O, and 24 mg of Co(NO₃)₂·6H₂O were firstly dispersed and dissolved in 35 mL of DMF. Then, 21 mg of 1,4-BDC was added to the suspension. After stirring for 15 min, a certain amount of ethanol, distilled water, and TEA were added. The solution was stirred for 12 h at room temperature. Finally, the product was collected by centrifugation at 1000 rpm, washed with a mixture of ethanol and water to remove impurities (mostly the unanchored MOF nanosheets; note that the unanchored 2D MOF was still dispersible in solution at a centrifugation speed below 1000 rpm). Then, the obtained BTO@MOF-Fe/Co heterostructures were lyophilized. Using a similar procedure, the BTO@MOF-Co heterostructure was also prepared by only using Co(NO₃)₂·6H₂O in the synthesis.

1.4 Electrochemical measurements

Electrochemical tests were carried out in a KOH aqueous solution (1.0 M). First, the glassy carbon (GC) disc (area = 0.07 cm²) was polished with aluminum powder (Beijing Enokai Co., Ltd.). Then, 5 mg of the BTO@MOF electrocatalyst was dispersed in 500 μ L of ethanol, together with 0.5 mg of carbon black in a 0.05 wt.% Nafion solution (0.5 mL), to prepare a typical suspension of the catalyst. The suspension was sonicated and quantitatively transferred to the surface of the polished GC disc and dried in air. For comparison, 3.725 mg BTO, and 1.275 mg MOF were used to prepare the electrocatalysts following the same method.

All electrochemical measurements were performed at room temperature using a CH Instruments 760E electrochemical workstation with a three-electrode system (Austin, TX). The working electrode was a modified GC electrode (diameter 3 mm). Hg/HgO and Pt plates were used as the reference and the counter electrode, respectively. Before each measurement, all electrolytes were degassed with high-purity nitrogen. The linear scan voltammogram of different samples was measured at a scan rate of 10 mV s⁻¹. Electrochemical impedance spectroscopy (EIS) was collected at a scanning frequency of 0.1 - 10⁵ Hz, using a 5 mV sinusoidal AC jitter, under the open-circuit voltage of 0.65 mV, to evaluate the electrical resistance of the electrochemical system. In addition, all experiments were carried out under the same conditions, and the electrode potential relative to the saturated calomel electrode potential was converted into reversible hydrogen electrode (RHE) potential according to the Nernst equation: $E(\text{vs. RHE}) = E(\text{vs. HgO}) + E_{\text{HgO}} + 0.0591 \text{ pH}$.

1.5 Other characterization

The crystalline structures of BaTiO₃ NPs and BaTiO₃@MOF heterojunctions were studied using X-ray diffraction (XRD, Bruker, D8 FOCUS) with Cu K α (1.5418 Å) as the source. Raman spectra were collected using a Reflex Raman spectrometer equipped with a 532 nm laser as the excitation source. The chemical composition was analyzed using X-ray photoelectron spectroscopy (XPS) with a Kratos Axis Ultra DLD spectrometer employing a monochromated Al K α X-ray source (1486.6 eV). Fourier transform infrared (FTIR) spectra were recorded using a Thermo Nicolet 6700 FTIR spectrometer using KBr pellets. Thermal degradation was carried out by thermogravimetric analysis (TGA, PerkinElmer Pyris 1) at a heating rate of 10 °C/min from 20 to 800 °C. Phase transitions were studied using differential scanning calorimetry (DSC, TA Instruments Discovery 250) at a heating rate of 10 °C.

The morphology of samples was characterized by scanning electron microscopy (SEM, FEI Nova Nano SEM 450) and field-emission transmission electron microscope (TEM, FEI Tecnai G2 F20). The TEM samples were prepared as follows. The BaTiO₃ NPs were dispersed in ethanol under ultrasonication and drop-cast onto a conductive silicon wafer substrate to form a monolayer. The substrate was transferred into the focused ion beam (FIB)-SEM vacuum chamber for observation and sampling. The appropriate position for sampling was selected through the SEM observation. A thin Pt layer (~200 nm) was firstly deposited by electron beam to fix the BTO NPs on the silicon wafer, and another Pt layer (~800 nm) was deposited by ion beam to

protect the sample spot. Then, the ion beam was adjusted to the cutting mode and grooves were made on both sides of the sampling area. After the thickness of the sample reached a certain value, it was cut and welded on the nanoarm for transfer. The sample was transferred to a 400-mesh copper grid and firmly welded, and then was thinned by ion beam to a thickness that could be suitable for high-resolution TEM study.

Broadband dielectric spectroscopy (BDS) measurement was carried out using a Novocontrol Concept 80 broadband dielectric spectrometer (Novocontrol Technologies, Montabaur, Germany) with temperature control. BaTiO₃ NPs were mixed with the silicone rubber at an 80/20 volume ratio. The BaTiO₃-silicone rubber mixture was cured at 80 °C in a vacuum oven overnight. BaTiO₃-silicone rubber pellets were pressed with a hydraulic press at a force of up to 2 ton (about 3.8 MPa). The packing fraction of BaTiO₃ NPs in the pellets was calculated based on the densities of BaTiO₃ (6.02 g/cm³) and silicone rubber (1.07 g/cm³), and TGA measurements. The applied voltage was 1.0 V_{rms} (i.e., root-mean-square voltage) with frequency ranging from 1 Hz to 1 MHz and temperature from -50 to 150 °C. Gold (Au) electrodes with an area of 7.06 mm² were evaporated on both surfaces of samples using a Quorum Q300T D Plus sputter coater (Quorum Technologies, Ltd., Laughton, East Sussex, UK). The Au electrode thickness was ca. 10 nm.

1.6 Density functional theory (DFT) calculation

The structure relaxation and single-point energies were calculated by the DFT calculations implemented in the Vienna Ab initio Simulation Package (VASP) procedure with the generalized gradient approximation (GGA) of Perdew-Burke-Ernzerhof (PBE). The related computational parameters were listed as the following: the plane wave cut-off energy was 400 eV, and the vacuum spacing in a direction perpendicular to the plane of the structure was 15 Å. The Brillouin zone integration was performed using 2×2×1 Monkhorst-Pack k-point sampling for a structure. The free energy was calculated using the equation: $G = E + ZPE - TS$, where E is the total energy, ZPE is the zero-point energy, T is the temperature in Kelvin (298.15 K used here), and S is the entropy.

2. XRD and Rietveld-fitting results of arBTO100, arBTO200, and anBTO200 NPs

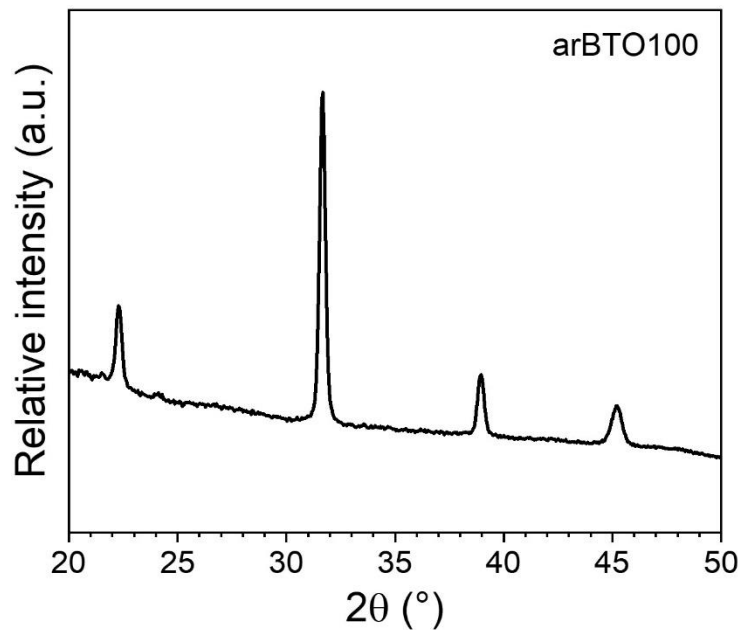


Fig. S1. One-dimensional XRD profile for the as-received 100 nm BaTiO₃ (arBTO100) nanoparticles at room temperature.

Table S1. Crystallographic data of Rietveld refinement for arBTO200 and anBTO200.

samples	arBTO200	anBTO200
crystal system	tetragonal	tetragonal
space group	P4mm	P4mm
a (Å)	3.9952	3.9948
b (Å)	3.9952	3.9948
c (Å)	4.0346	4.0357
cell volume(Å ³)	64.398	64.405
c/a	1.0098	1.0102

3. FTIR, TGA, and XRD results of arBTO200/anBTO200, 2D MOFs, and their heterostructures

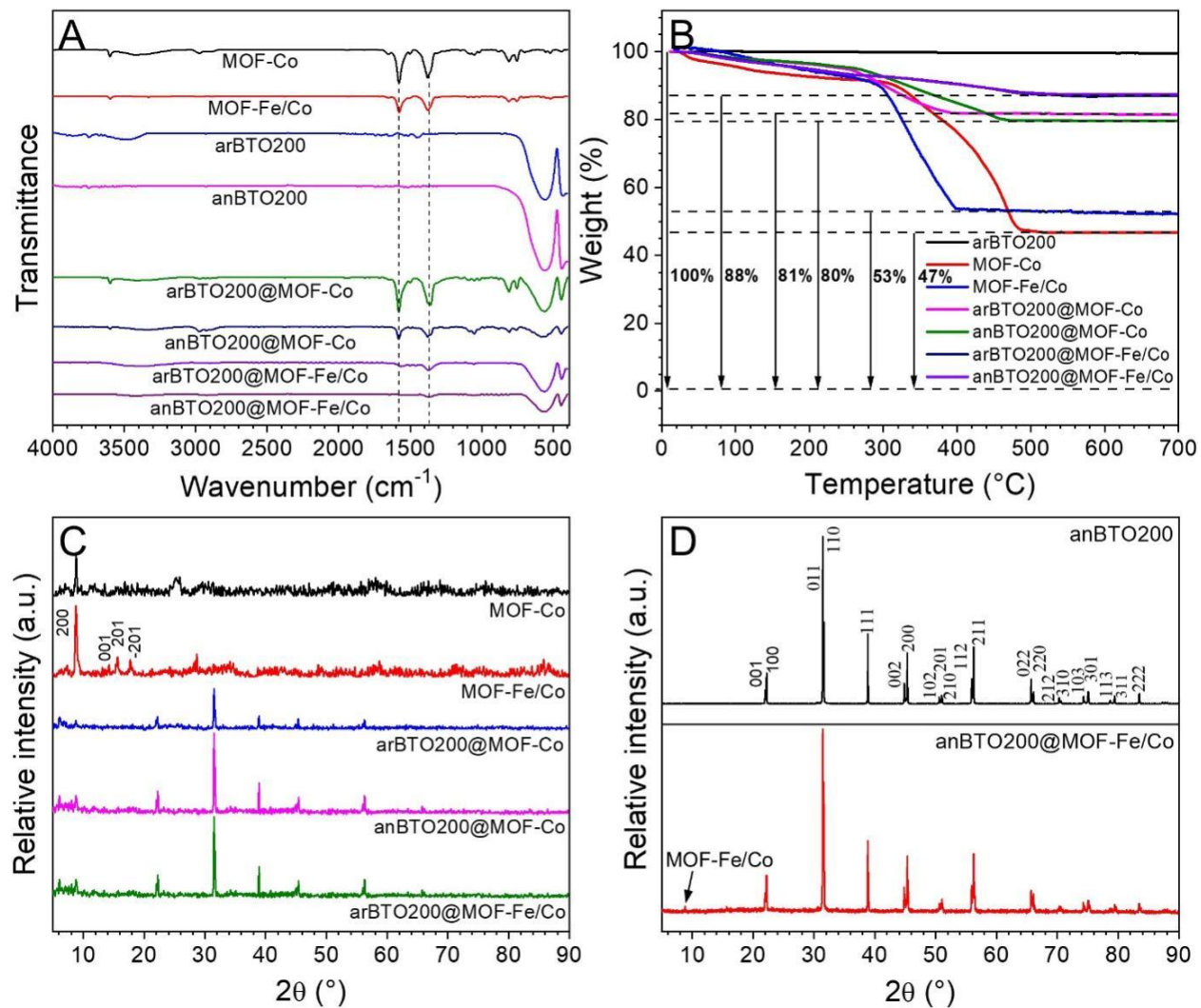


Fig. S2. (A) FTIR spectra, (B) TGA curves, and (C,D) XRD profiles of MOF-Co, MOF-Fe/Co, arBTO200, anBTO200, arBTO200@MOF-Co, anBTO200@MOF-Co, arBTO200@MOF-Fe/Co, and anBTO200@MOF-Fe/Co at room temperature.

4. XPS results of arBTO200 and anBTO200

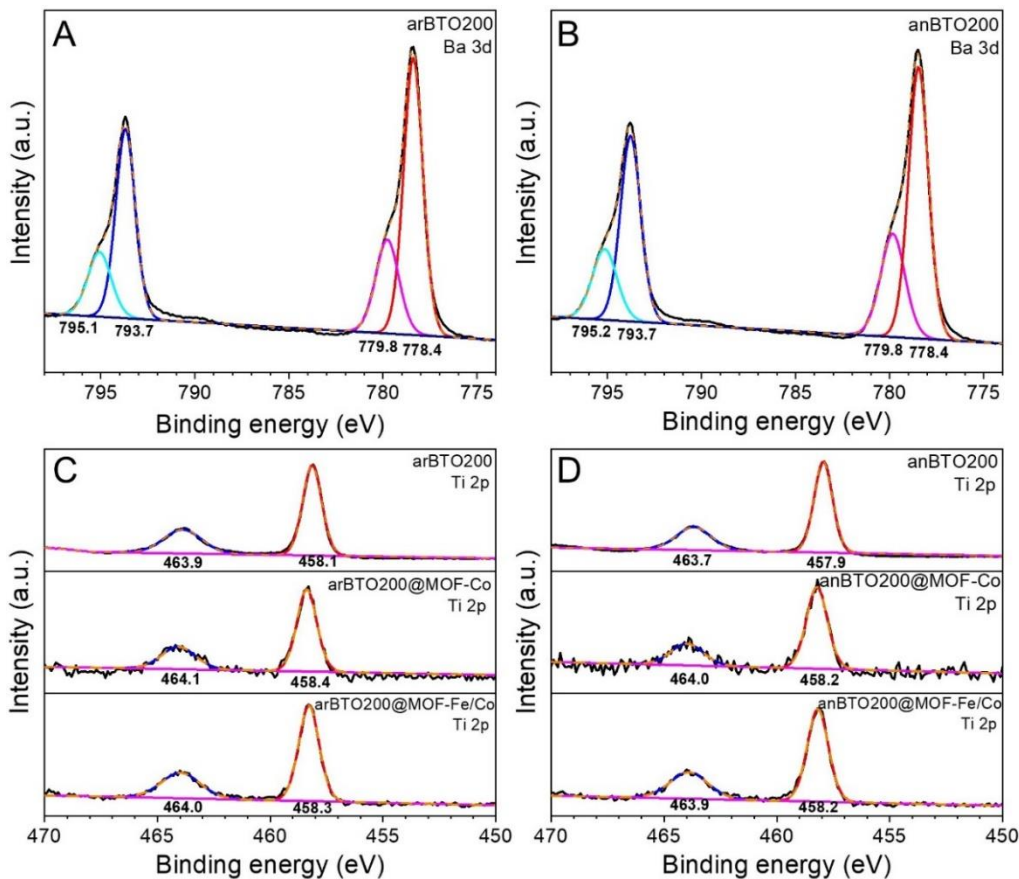


Fig. S3. XPS Ba 3d spectra of (A) arBTO200 and (B) anBTO200 NPs. XPS Ti 2p spectra of (C) arBTO200, arBTO200@MOF-Co, arBTO@MOF-Fe/Co and (D) anBTO200, anBTO200@MOF-Co, and anBTO200@MOF-Fe/Co.

5. Overpotential of different catalysts

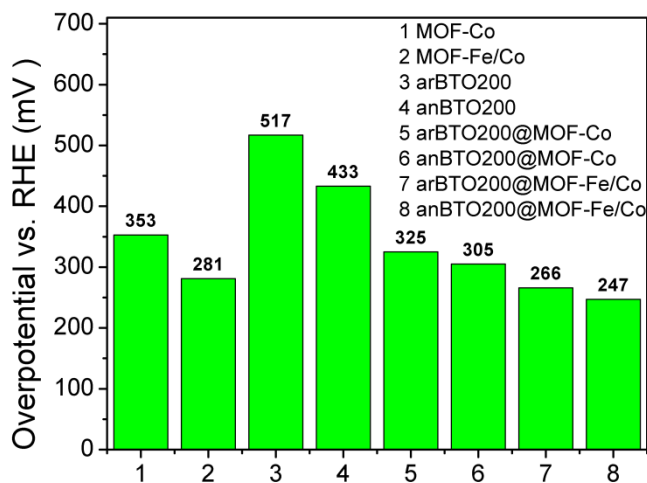


Fig. S4. Overpotential of different catalysts at 10 mA cm⁻² versus RHE.

6. CV curves of different catalysts

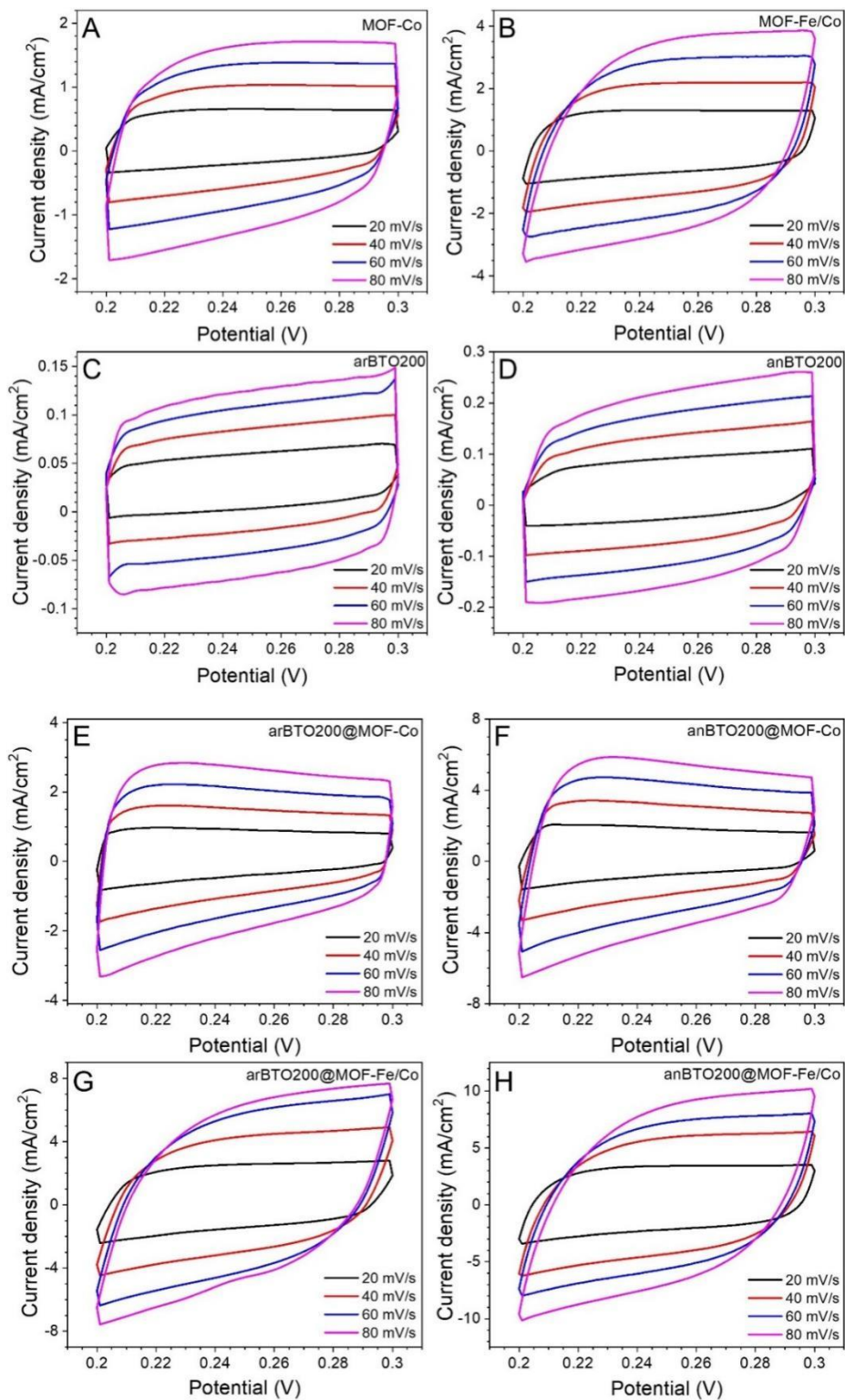


Fig. S5. CV curves in a potential range of 0.2-0.3 V for (A) MOF-Co, (B) MOF-Fe/Co, (C) arBTO200, (D) anBTO200, (E) arBTO200@MOF-Co, (F) anBTO200@MOF-Co, (G)

arBTO200@MOF-Fe/Co, and (H) anBTO200@MOF-Fe/Co.

7. Calculated ohmic contact resistances (R_s) and charge transfer resistance (R_{ct}) for different catalysts

Table S2. Calculated ohmic contact resistances (R_s) and charge transfer resistance (R_{ct}) from the equivalent circuit of different electrocatalyst.

Catalysts	R_s / Ω	R_{ct} / Ω
MOF-Co	12.27	78.96
MOF-Fe/Co	12.18	12.64
arBTO200	12.06	6357
anBTO200	11.98	6278
arBTO200@MOF-Co	12.01	97.87
anBTO200@MOF- Co	11.59	50.96
arBTO200@MOF- Fe/Co	11.93	11.53
anBTO200@MOF- Fe/Co	11.52	5.645

8. Durability of arBTO200@MOF-Fe/Co catalysts

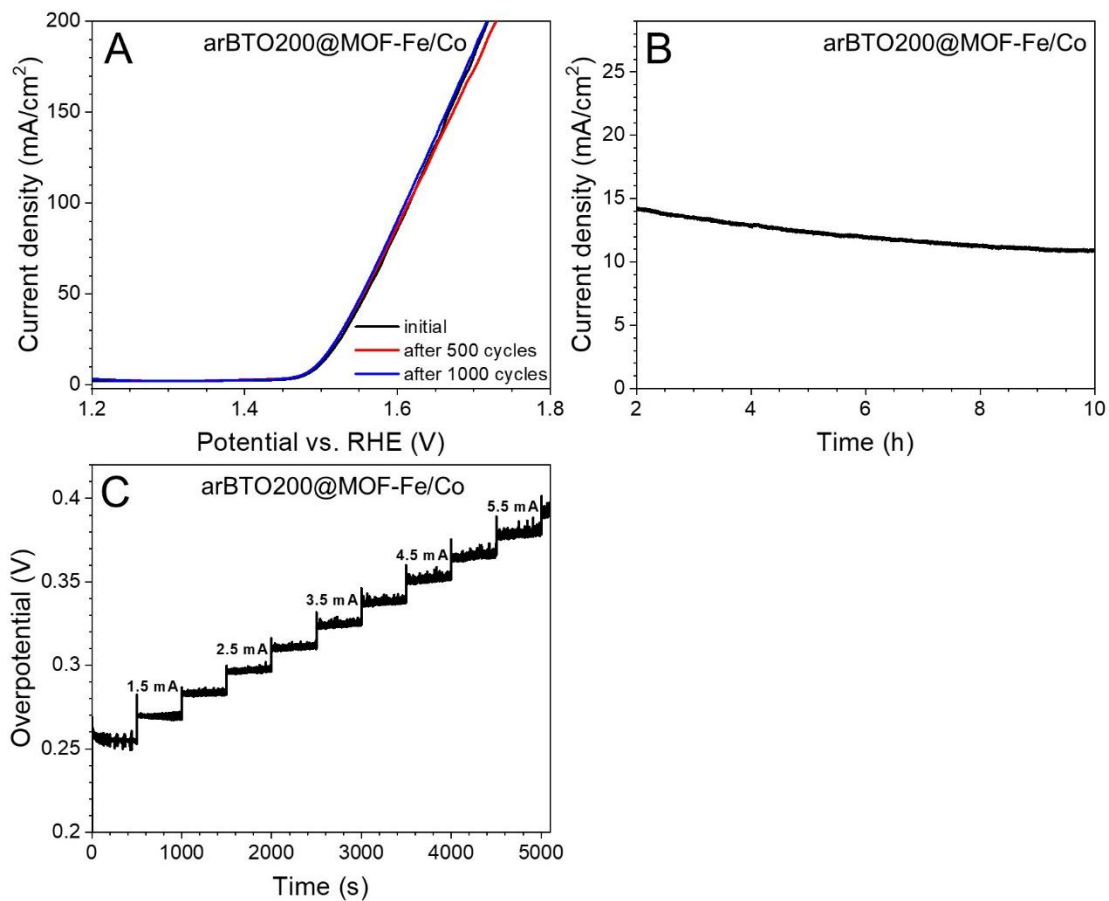


Fig. S6. Durability of arBTO200@MOF-Fe/Co catalyst. (a) Polarization curves for the arBTO200@MOF-Fe/Co catalyst in water. (b) Long time chronoamperometric response curve of the arBTO200@MOF-Fe/Co catalyst. (c) Multicurrent process with the current density increased from 1.0 to 5.5 mA.

9. SEM images of the catalyst after the OER stability test

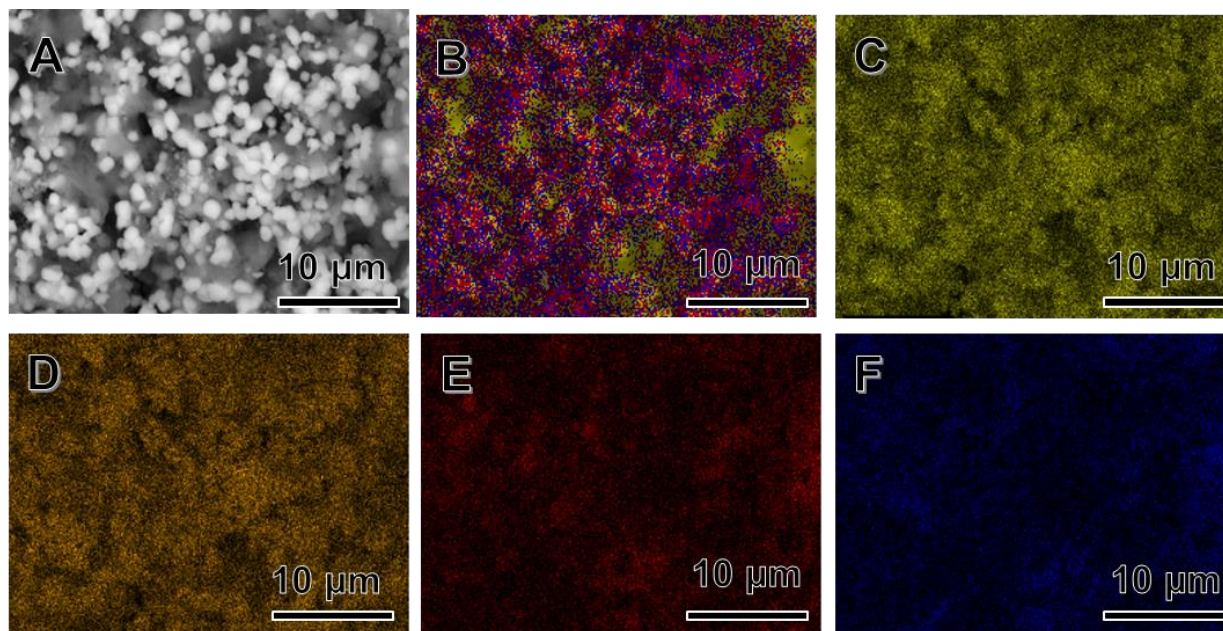


Fig. S7. SEM images of (A) anBTO@MOF-Fe/Co catalyst after the OER stability test. EDS elemental mapping images (B) for anBTO200@MOF-Fe/Co: (C) Ti, (D) Ba, (E) Fe, and (F) Co.

10. XRD results of the catalyst after the stability test

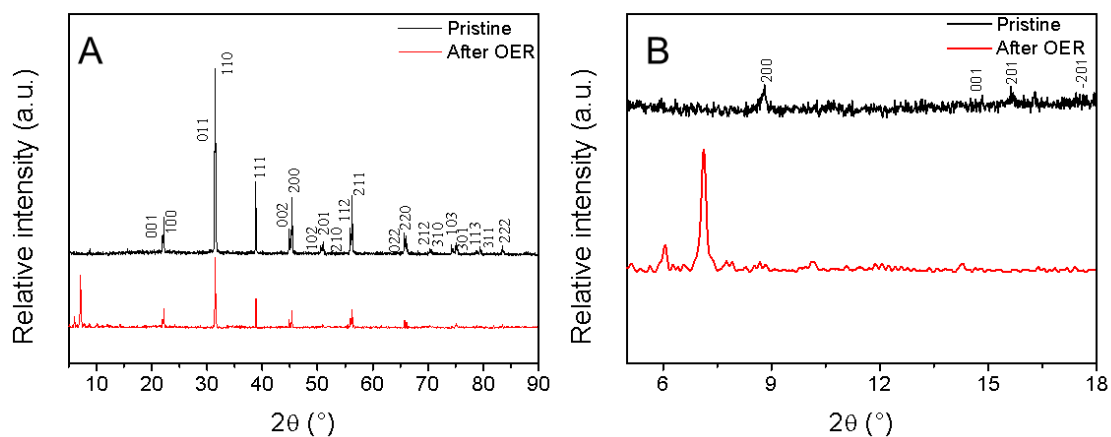


Fig. S8. XRD patterns (A) and the enlarged XRD patterns scanned within the 2θ range from 5° to 18° (B) of anBTO200@MOF-Fe/Co catalyst before and after the OER stability test.

11. XPS results of anBTO200@MOF-Fe/Co before and after the OER stability test

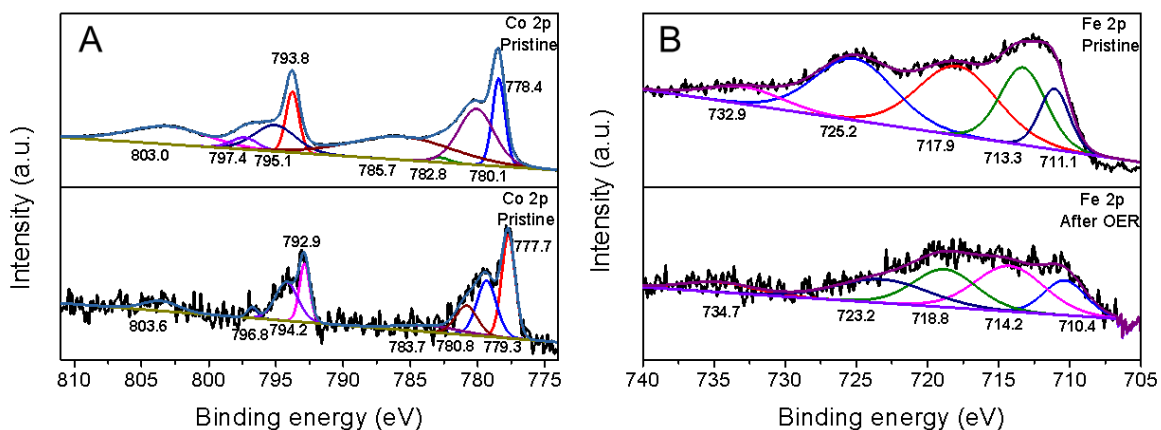


Fig. S9. High-resolution XPS spectra of Fe 2p (A) and Co 2p (B) of anBTO200@MOF-Fe/Co before and after the OER stability test.

12. Unit cell structures for the DFT calculations

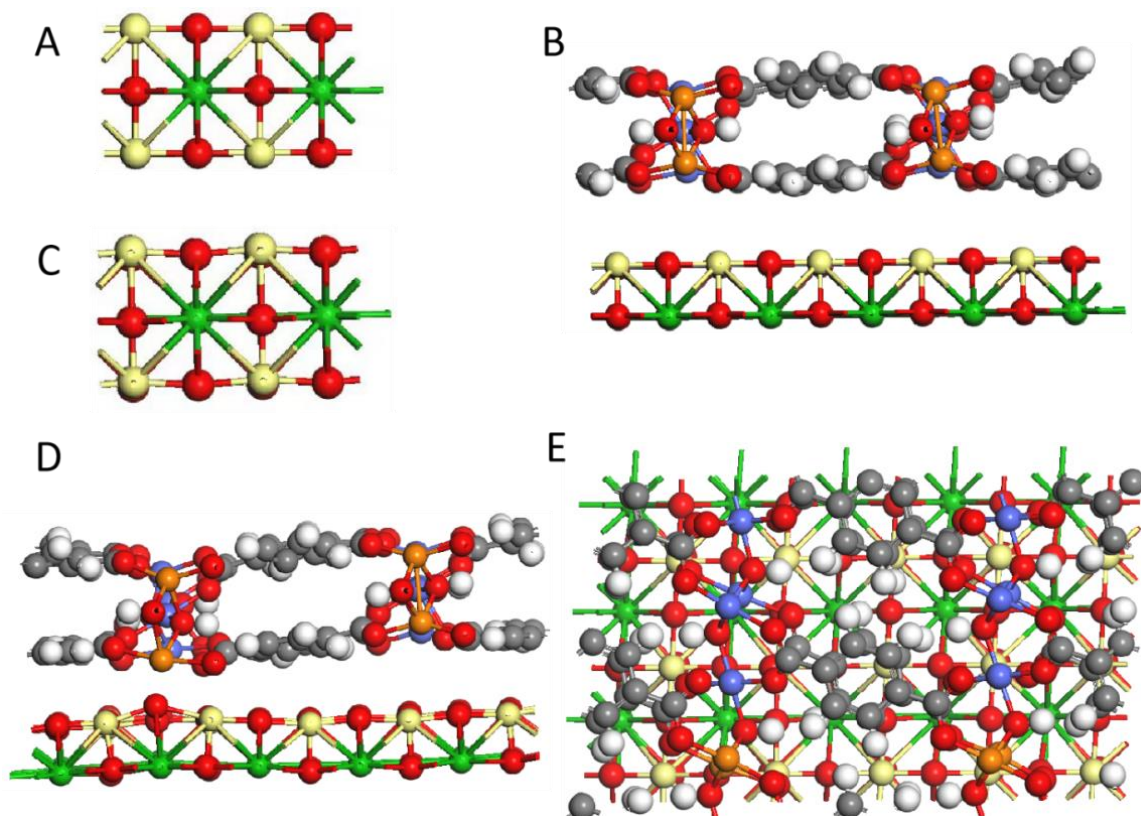
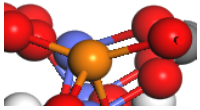
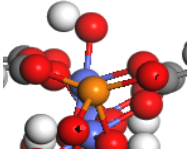
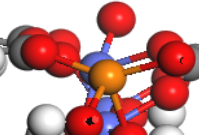
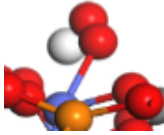
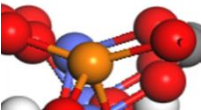


Fig. S10. Unit cell structures of (A) cubic BTO, (B) tetragonal BTO, (C) cubic BTO@MOF-Fe/Co in the front view, and tetragonal BTO@MOF-Fe/Co crystal structure in the (D) front and (E) top views. Color code: Ba (green), Ti (yellow), O (red), Fe (brown), Co (blue), C (gray), H (white).

Table S3. Unit cell diagrams of reaction sites in Co and Fe in Fe/Co MOF, respectively.

	OH^-	OH^*	O^*	OOH^*	O_2
Reaction site of Co					
Reaction site of Fe	